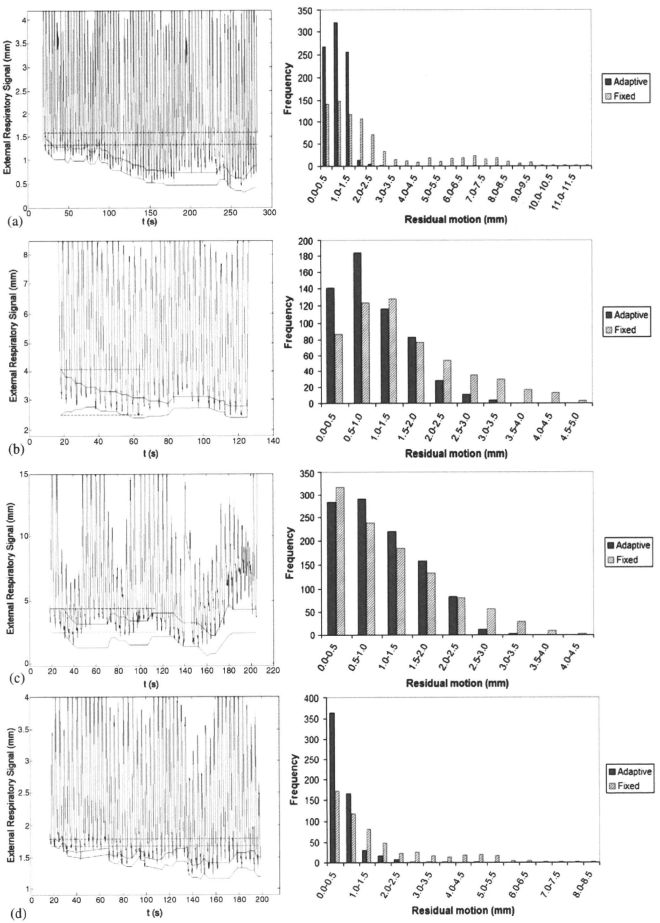

Figure 4. Four different treatment fractions showing the external signal (left) with the fixed (dotted line) and adaptive (continuous line) gating windows. The length of the fixed gating window signifies the duration of beam-on time. The residual tumor motion for the respective gating windows (right) is also shown.

Table 2. A summary of all the measurements made for the fixed and adaptive gating window techniques.

	R95 (mm)		DC (%)		RG3 (%)		MXR (mm)	
Patient	Fixed	Adaptive	Fixed	Adaptive	Fixed	Adaptive	Fixed	Adaptive
1†	2.1 ± 0.1	1.9 ± 0.1	57 ± 7	54 ± 7	0.3 ± 0.4	0.03 ± 0.04	3.4	3.1
2†	2.3 ± 0.7	1.9 ± 0.3	43 ± 8	33 ± 11	2.1 ± 3.2	0.3 ± 0.3	4.4	3.9
3	2.2 ± 0.5	2.6 ± 0.4	31 ± 28	19 ± 6	0.3 ± 0.4	0.9 ± 0.9	3.2	3.7
4	2.6 ± 0.8	2.2 ± 0.8	42 ± 13	34 ± 13	4.3 ± 6.1	2.1 ± 4.2	5.1	4.7
5	2.9 ± 1.1	4.7 ± 2.9	17 ± 11	9 ± 3	7.2 ± 12.6	13.5 ± 15.2	4.9	20.3
6†	3.0 ± 0.8	2.5 ± 0.6	33 ± 12	19 ± 4	6.8 ± 6.9	2.2 ± 4	5.6	4.3
7†	2.0 ± 0.4	1.8 ± 0.3	36 ± 7	29 ± 8	0.5 ± 0.7	0.3 ± 0.9	4.2	4.2
8†	2.9 ± 1.7	1.8 ± 0.7	12 ± 8	15 ± 9	6.5 ± 7.6	1.5 ± 3.1	11.6	6.8
Average	2.5	2.4	33.8	26.5	3.5	2.6	5.3	6.4

† Indicates statistically significant difference in R95 between the fixed and adaptive gating techniques. The p-values for patients 1, 2, 6, 7 and 8 are 0.012, 0.003, 0.002, 0.010 and 0.011, respectively.

technique for six out of eight patients. It was interesting to note that the data from two patients (3 and 5) were the ones that consistently showed a worse performance with the adaptive gating technique. We observed that some of the fractions (particularly for patients 3 and 5) used for this analysis had highly irregular breathing patterns, as the one shown in figure 4(c). Since the adaptive gating technique was designed specifically to track smooth changes in the breathing pattern (such as the baseline drifts shown in figures 4(a) and (d)) it did not perform well with some of the abrupt changes in the highly irregular breathing patterns.

After a closer examination of all the breathing patterns, we went through the analysis again by leaving out certain cases of highly irregular breathing patterns, under the assumption that patients under breath coaching would breathe relatively normally (Neicu *et al* 2006, Kini *et al* 2003). This resulted in leaving out patients 3 and 5 as well as fractions 8 (figure 4(c)), 1 and 6 from patients 2, 4 and 7, respectively, and fractions 2, 3, 4, 6, 7 and 14 from patient 8. The remaining data reflected more stable or smoothly varying breathing patterns. Figure 5 summarizes the results of the remaining patients, after leaving out the fractions with highly irregular breathing cycles.

Figure 5 shows that for all six patients R95 was reduced with the difference being statistically significant in all six cases (p-value < 0.025). On average, R95 was reduced by 24% with the adaptive gating window technique, going from 2.5 mm with the fixed gating window technique to 1.9 mm. The average R95 was larger than 3 mm for two patients (6 and 8*) for the fixed gating window, while for the adaptive gating window the largest average R95 was 2.5 mm. The DC was lower for all but one patient for the adaptive gating window with the average being 31% versus 38.5%. In total, the DC was greater than 20% for 42 out of 52 fractions for the fixed and 39 out of 52 fractions for the adaptive gating window techniques. The variations in the DC were quite large, with the fixed gating window ranging from 15% to 57%, while with the adaptive gating window ranging from 16% to 54%. The percentage of beam-on time that resulted in residual tumor motion greater than 3 mm was lower for all six cases for the adaptive gating technique. The maximum average value for the adaptive gating technique was only about 2% (patient 6) while reaching 8% (patient 8*) for the fixed gating window technique.

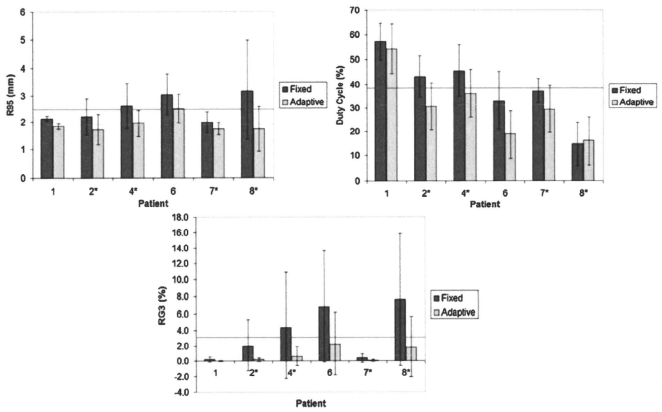

Figure 5. A plot of the residual motion (R95), DC and percent above 3% (RG3) for each patient and each gating technique (fixed and adaptive). The error bars on each plot reflect the standard deviation. The solid line indicates the mean of all fractions for the fixed gating technique and the dotted line the mean of all fractions for the adaptive gating technique. *Irregular breathing patterns excluded.

4. Discussion

Respiratory gating for radiation therapy as implemented in our clinic resembles the fixed gating window technique simulated in this study. If there is no information about the position of the tumor during treatment two main issues arise: baseline drifts and time shifts. There is no way of dealing with these issues without disruption of the treatment process. Baseline drifts could be identified by monitoring the breathing trace, but before the treatment is interrupted to re-adjust the gating window, several MUs could be delivered at the wrong phase of the breathing cycle. Furthermore, even if a baseline drift is identified on time, it can cause delays in the treatment, since the treatment has to be stopped and the internal/external signal correlation must be reassessed. In addition, the time shifts cannot be identified unless there is information about the position of the tumor during treatment. The lack of monitoring means uncertainty, which can result in large residual motion and consequently in marginal misses.

Several studies have investigated updating of the internal/external correlation during treatment (Schweikard *et al* 2000, Kanoulas *et al* 2007, Wu *et al* 2008). Schweikard *et al* (2000), utilizing the CyberKnife system, update the internal/external correlation between a marker placed on the patient's abdomen and periodic x-ray images taken every 10 s. Kanoulas *et al* (2007) investigated the updating of the correlation based on a pair of radiographic images taken at a fixed frequency during treatment. Both methods result in an extra dose from kV and they do not necessarily monitor what would happen during beam-on time, in a gated treatment. Our approach is similar to the approach taken by Wu *et al* (2008) in that it is specifically designed for respiratory gating. In their study, the internal/external correlation updating happens from information obtained during the beam-on time; however, it is based on information obtained from a single image.

The method we propose utilizes beam's-eye-view images obtained during the entire beam-on time. In addition with our method the residual motion is directly measured and the gating window is adapted with the goal to keep the residual motion below a certain level and not just to correlate internal and external signals. The results illustrate that updating the gating window based on information obtained during the previous beam-on time may give enough information to successfully track the end-exhale position, and follow smooth baseline drifts. With our method the correlation of the internal and external signals is not directly updated during treatment. The issue of changing correlation is dealt with in an indirect manner by compensatory widening and narrowing of the gating window. There could be cases in which the time shift is so large that the residual motion cannot be kept below 3 mm, without having a significantly reduced DC. In such cases the efficacy of gating using external surrogates should be reassessed and alternate treatment methods might be more appropriate. In general, with the adaptive gating technique the DC was reduced; however it was still acceptable with an average of 27% for all eight patients.

Apart from the reduction in the DC, another disadvantage of the adaptive gating window technique is that it relies on tracking the tumor on MV and kV images. That tracking can also be associated with an uncertainty, which the fixed gating window technique does not have, and has to be included in planning. However, with the adaptive gating window technique the allowed residual tumor motion is chosen before the treatment (in this case it was 3 mm) and as the top left plot of figure 5 illustrates, R95 can be kept below that goal for all of the patients. The added level of reliability could result in a reduction of the safety margins.

There was a statistically significant reduction in the DC (p-value $= 0.012$) going from the fixed to the adaptive gating window technique. We investigated whether the reduction in the residual tumor motion was purely a consequence of the reduced DC. The residual tumor motion, R95, was calculated only for the cases where the adaptive gating technique resulted in an increase in the DC. A total of 22 fractions were included in that analysis. It was found that while there was a statistically significant increase (p-value < 0.001) in the DC (15 to 19% on average) there was also a decrease in the residual tumor motion (from 2.5 to 1.9 mm on average), with a borderline significant t-test result (p-value $= 0.046$). In addition, the correlation between the change in the DC and the change in the residual tumor motion between the fixed and adaptive gating window techniques was close to zero (0.09) for all the fractions. Combining these results points to the fact that the reduction in R95 was a product of tumor tracking during treatment. Moreover, even if some of the reduction in the R95 came from a reduction in the DC that would have been necessitated by the algorithm to keep the residual motion low, which is the ultimate goal.

The available data were taken from the patients breathing freely, which resulted in breathing patterns for some treatment fractions that had highly variable breathing periods, drifting and variable peak-to-peak amplitudes. By leaving out these highly irregular breathing patterns we showed that the residual tumor motion could be reduced for the adaptive gating technique (2.4 mm to 1.9 mm), but not for the fixed gating window (2.5 mm for both). This suggests that the image-guided adaptive gating technique needs to be combined with breath coaching in order to be more effective. It also suggests that breath coaching alone cannot help reduce residual motion. Residual tumor motion is significantly lower for the adaptive gating window technique for all patients with more regular breathing patterns. In addition, the percentage of time that the residual motion is above 3 mm is quite low for the adaptive gating window, with the maximum average value being only 2% for all the patients. This suggests not only that the residual tumor motion is reduced overall, but also that it is done in a more reliable manner, since it results in only a few instances having residual motion larger than 3 mm.

5. Conclusions

The computer simulation study presented with this work demonstrates how information obtained with the imaging (kV/MV) performed under our current clinical gating protocol could be utilized to track the exhale tumor position before and during treatment. The result is an adaptive gating window that leads to a decrease in the residual tumor motion, as demonstrated using real patient data. This is based on the assumption that fast and reliable algorithms can be employed for direct tumor tracking on both MV and kV images. The evolution of research in this field suggests that the clinical realization of this may not be far in the future. With kV/MV imaging and real-time image processing, image-guided adaptive gating can result in consistent reduction of the residual tumor motion, which in turn could facilitate the reduction of margins used to account for tumor motion.

References

Adamson J *et al* 2008 Prostate intrafraction motion evaluation using kV fluoroscopy during treatment delivery: a feasibility and accuracy study *Med. Phys.* **35** 1793–806

Arimura H *et al* 2009 Computerized method for estimation of the location of a lung tumor on EPID cine images without implanted markers in stereotactic body radiotherapy *Phys. Med. Biol.* **54** 665–77

Arriagada R *et al* 1991 ASTRO (American Society for Therapeutic Radiology and Oncology) plenary: effect of chemotherapy on locally advanced non-small cell lung carcinoma: a randomized study of 353 patients. GETCB (Groupe d'Etude et Traitement des Cancers Bronchiques), FNCLCC (Féderation Nationale des Centres de Lutte contre le Cancer) and the CEBI trialists *Int. J. Radiat. Oncol. Biol. Phys.* **20** 1183–90

Berbeco R I *et al* 2005 Residual motion of lung tumours in gated radiotherapy with external respiratory surrogates *Phys. Med. Biol.* **50** 3655–67

Berbeco R I *et al* 2007 Clinical feasibility of using an EPID in CINE mode for image-guided verification of stereotactic body radiotherapy *Int. J. Radiat. Oncol. Biol. Phys.* **69** 258–66

Berbeco 2009 Marker-less verification of respiratory-gated radiotherapy for lung cancer *Med. Phys.* **36** 2491

Chi P *et al* 2006 Relation of external surface to internal tumor motion studies with cine CT *Med. Phys.* **33** 3116–23

Cho B *et al* 2009 First demonstration of combined kV/MV image-guided real-time dynamic multileaf-collimator target tracking *Int. J. Radiat. Oncol. Biol. Phys.* **74** 859–67

Curran W J *et al* 2003 Long-term benefit is observed in a phase III comparison of sequential versus concurrent chemo-radiation for patients with unresected stage III NSCLC: RTOG 9410 *Proc. Am. Soc. Clin. Oncol.* **22** 2499 (abstract)

D'Souza W D *et al* 2005 Real-time intra-fraction-motion tracking using the treatment couch: a feasibility study *Phys. Med. Biol.* **50** 4021–33

Ford E C *et al* 2003 Respiration-correlated spiral CT: a method of measuring respiratory-induced anatomic motion for radiation treatment planning *Med. Phys.* **30** 88–97

Hugo G *et al* 2006 Changes in the respiratory pattern during radiotherapy for cancer in the lung *Radiother. Oncol.* **78** 326–31

Ionascu D *et al* 2007 Internal–external correlation investigations of respiratory induced motion of lung tumors *Med. Phys.* **34** 3893–903

Jemal A *et al* 2009 Cancer statistics *CA Cancer J. Clin.* **59** 225–49

Kanoulas E *et al* 2007 Derivation of the tumor position from external respiratory surrogates with periodical updating of the internal/external correlation *Phys. Med. Biol.* **52** 5443–56

Kini V R *et al* 2003 Patient training in respiratory-gated radiotherapy *Med. Dosim.* **28** 7–11

Kontrisova K *et al* 2006 Dosimetric comparison of stereotactic body radiotherapy in different respiration conditions: a modeling study *Radiother. Oncol.* **81** 97–104

Korreman S S *et al* 2008 Respiratory gated beam delivery cannot facilitate margin reduction, unless combined with respiratory correlated image guidance *Radiother. Oncol.* **86** 61–8

Lin T *et al* 2009 Markerless gating for lung cancer radiotherapy based on machine learning techniques *Phys. Med. Biol.* **54** 1555–63

Mao W *et al* 2008 A fiducial detection algorithm for real-time image guided IMRT based on simultaneous MV and kV imaging *Med. Phys.* **35** 3554–64

Meyer J *et al* 2006 Tracking moving objects with megavoltage portal imaging: a feasibility study *Med. Phys.* **33** 1275–80

Murray B *et al* 2007 Frame-based immobilization and targeting for stereotactic body radiation therapy *Med. Dosim.* **32** 86–91

Neicu T *et al* 2006 Synchronized moving aperture radiation therapy (SMART): improvement of breathing pattern reproducibility using respiratory coaching *Phys. Med. Biol.* **51** 617–36

Nishioka S *et al* 2008 Exhale fluctuation in respiratory-gated radiotherapy of the lung: a pitfall of respiratory gating shown in a synchronized internal/external marker recording study *Radiother. Oncol.* **86** 69–76

Nottrup T J *et al* 2007 Intra- and interfraction breathing variations during curative radiotherapy for lung cancer *Radiother. Oncol.* **84** 40–48

Papiez L *et al* 2005 Real-time DMLC IMRT delivery for mobile and deforming targets *Med. Phys.* **32** 3037–48

Purdie T G *et al* 2007 Cone-beam computed tomography for on-line image guidance of lung stereotactic radiotherapy: localization, verification, and intrafraction tumor position *Int. J. Radiat. Oncol. Biol. Phys.* **68** 243–52

Rottmann J *et al* 2009a Mutual information for beams-eye-view lung tumor tracking without radiopaque markers *Med. Phys.* **36** 2431

Rottmann J *et al* 2009b Multi-region tracking for lung tumor motion assessment *Int. Conf. on Machine Learning and Applications* pp 489–93

Schweikard A *et al* 2000 Robotic motion compensation for respiratory movement during radiosurgery *Comput. Aided Surg.* **5** 263–77

Sonke J *et al* 2005 An off-line 4D cone beam CT based correction protocol for lung tumor motion *Int. J. Radiat. Oncol. Biol. Phys.* **63** S389–90

Vedam S *et al* 2001 Determining parameters for respiration-gated radiotherapy *Med. Phys.* **28** 2139–46

Wiersma R D *et al* 2008 Combined kV and MV imaging for real-time tracking of implanted fiducial markers *Med. Phys.* **35** 1191–8

Wu *et al* 2008 Gating based on internal/external signals with dynamic correlation updates *Phys. Med. Biol.* **53** 7137–50

Xu Q *et al* 2008 Lung tumor tracking in fluoroscopic video based on optical flow *Med. Phys.* **35** 5351–9

IOP Publishing Physics in Medicine and Biology

Phys. Med. Biol. **55** (2010) 3325–3337 doi:10.1088/0031-9155/55/12/005

Site-specific volumetric analysis of lung tumour motion

Eric W Pepin[1], Huanmei Wu[2], George A Sandison[3], Mark Langer[4] and Hiroki Shirato[5]

[1] School of Health Sciences, Purdue University, West Lafayette, IN 47907, USA
[2] Purdue School of Engineering and Technology, IUPUI, Indianapolis, IN 46202, USA
[3] Department of Radiation Oncology, University of Washington, Seattle, WA 98195, USA
[4] Indiana University School of Medicine, Indianapolis, IN 46202, USA
[5] Hokkaido University School of Medicine, Sapporo, Japan

E-mail: epepin@purdue.edu

Received 2 February 2010, in final form 13 April 2010
Published 26 May 2010
Online at stacks.iop.org/PMB/55/3325

Abstract

The treatment of lung cancer with radiation therapy is hindered by respiratory motion. Real-time adjustments to compensate for this motion are hampered by mechanical system latencies and imaging-rate restrictions. To better understand tumour motion behaviour for adaptive image-guided radiation therapy of lung cancer, the volume of a tumour's motion space was investigated. Motion data were collected by tracking an implanted fiducial using fluoroscopy at 30 Hz during treatment sessions. A total of 637 treatment fractions from 31 tumours were used in this study. For each fraction, data points collected from three consecutive breathing cycles were used to identify instantaneous tumour location. A convex hull was created over these data points, defining the tumour motion envelope. The study sought a correlation between the tumour location in the lung and the convex hull's volume and shape. It was found that tumours located in the upper apex had smaller motion envelopes (<50 mm^3), whereas tumours located near the chest wall or diaphragm had larger envelopes (>70 mm^3). Tumours attached to fixed anatomical structures had small motion spaces. Three general shapes described the tumour motion envelopes: 50% of motion envelopes enclosed largely 1D oscillation, 38% enclosed an ellipsoid path, 6% enclosed an arced path and 6% were of hybrid shape. This location–space correlation suggests it may be useful in developing a predictive model, but more work needs to be done to verify it.

(Some figures in this article are in colour only in the electronic version)

1. Introduction

In the administration of radiation therapy for lung cancer tumours, accurate dose delivery is challenged by respiratory-induced intra-fractional tumour motion (Keall *et al* 2006); this is

of particular importance in hypofractionated stereotatic radiosurgery. In one study, 50% of tumours had motion of at least 5 mm and 11% had motion greater than 10 mm (Chang *et al* 2008). This motion reduces the accuracy of the treatment and increases the uncertainty in the delivered dose, particularly when the motion extent is 1 cm or more (Keall *et al* 2001, Bortfeld *et al* 2002, Jiang *et al* 2003).

Tumour motion can be tracked accurately in real time, using techniques such as monitoring the anterior abdominal surface (Haasbeek *et al* 2007) or implanted fiducials (Shirato *et al* 2000). Such monitoring enables advanced image-guided radiation treatment of moving tumours, including the gated treatment delivery (RPM, Varian Medical Systems, Palo Alto, CA) and tumour tracking (CyberKnife Synchrony, Accuray, Sunnyvale, CA) (Haasbeek *et al* 2007, Smith *et al* 2009, Putra *et al* 2008, Ruan *et al* 2006, Vedam *et al* 2004). All the advanced motion compensation methods require an adequate understanding of motion characteristics. For example, in beam tracking, the important parameters of the tumour trajectory must be quantified to be used in treatment planning. Furthermore, these quantities must be continually monitored during treatment to ensure proper treatment delivery. Even though the precise three-dimensional (3D) locations of a moving tumour can be available in real time, radiation treatment delivery adjustments are hindered by mechanical system latencies and imaging-rate restrictions. The characterization of intra-fractional tumour motion helps the design of appropriate treatment approaches and enables the development of a predictive tumour motion behaviour model facilitating real-time image-guided radiation therapy (IGRT) of patients with free breathing during treatment.

Previous studies have focused on breathing characteristics such as amplitude and tidal volume (Yang *et al* 2008, Low *et al* 2005, Hoisak *et al* 2006, Chol *et al* 2008, Ren *et al* 2007, McCall and Jeraj 2007, Putra *et al* 2008, Wu *et al* 2007) for their descriptions of breathing behaviour, while mathematical models have been constructed using autoregressive moving averages (Ren *et al* 2007, McCall and Jeraj 2007) and combinations of periodic and semi-periodic functions (Putra *et al* 2008). The prediction models in these studies have had limited dependences on parameters related to tumour location in the lung and have lacked an overall description of tumour motion. The total volume occupied during breathing phases was investigated as the internal gross tumour volume (IGTV) (Kang *et al* 2007) using four-dimensional computed tomography (4DCT). Handels *et al* also calculated motion volume in this manner (Handels *et al* 2007). These volumes, however, are dependent on tumour volume and may not indicate the extent of tumour motion. The present study differs in that the volumes derived are indicative of real tumour motion.

This study is to investigate the relationship of tumour location in the lungs and motion characteristic, focusing on the space encompassed by lung tumours during treatment. We investigated the correlation between the size and shape of the tumour motion space with the location and attachment status of the tumour. Identified correlations may provide additional parameters useful in the development of a robust predictive model for future tumour motion in real-time adaptive IGRT.

2. Method and materials

2.1. Materials

This study used the 3D motion of implanted gold fiducials in 31 lung tumours during 637 radiotherapy fractions (ranged from 6 to 44 fractions per tumour) tracked using real-time fluoroscopy at a rate of 30 Hz at Hokkaido University (Shirato *et al* 2000). For each fraction, the motion of the tumour during the first three consecutive breathing cycles was studied. A

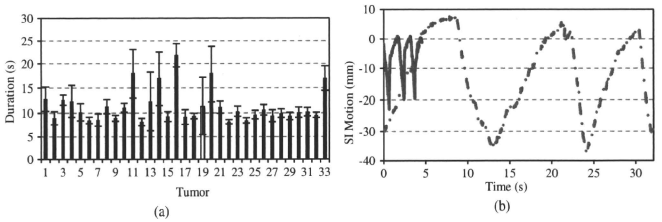

Figure 1. Data set durations. (a) For each tumor, the total duration of the three-breathing-cycle data set used in the analysis was averaged over all treatment fractions. Error bars show the standard deviation of all fractions. (b) The shortest three-breathing-cycle data set has 137 data points or 4.57 s (solid curve). The longest three-breathing-cycle data set has 964 data points or 32.1 s (dashed curve).

breathing cycle lasts about 3 to 5 s, and the average three-breathing-cycle data set size was 340 points. The cycle duration averaged over all treatment fractions for each patient is shown in figure 1(a).

The breathing cycle durations not only change from patient to patient but also from fraction to fraction, and even from one cycle to the next. The shortest and the longest three-breathing-cycle data sets are illustrated in figure 1(b). Incidentally, these are two different treatment sessions for the same tumor, as indicated by the white bar in (a). For one fraction, the breathing is fast and shallow, giving a total duration of 4.6 s for three cycles. For the other fractions, the breathing is slow and deep, giving a total duration of 32 s for three cycles. The figure also demonstrates intra-fractional inter-cyclic variations.

2.2. *Methods*

The motion envelope of the tumour in 3D space is calculated based on assigning a tumour position to a single point. This point was the position of one implanted fiducial in each tumour. Studies have shown the fiducial positions to be robust against migration (Kitamura *et al* 2002, Hashimoto *et al* 2005, Imura *et al* 2005, Shirato *et al* 2006, Katoh *et al* 2008, Onimaru *et al* 2005). The following three steps were used in the site-specific volumetric analysis of lung tumour motion.

(i) Outlier removal. Qualitatively, outliers can be defined as points that are physically separated from most other points and whose removal would substantially alter the size and/or shape of the motion envelope. Two criteria are proposed to identify outlier data points: one is based on motion velocity and the other is based on data point density. Motion velocity is limited by the patient's breathing frequency and amplitude. With an imaging rate of 30 Hz, fiducial displacement between frames is constrained by velocity. Furthermore, such a frequency makes it unlikely that the local neighbourhood of a fiducial position would not contain points collected in temporal proximity. Nakayama reported a maximum tumour velocity of 95.1 mm s^{-1} (Nakayama *et al* 2008).

Velocity-based outlier removal. The instantaneous velocity of the fiducial at each point was determined by dividing the absolute 3D Euclidean distance to it from the previous point by 1/30 s. Points were identified as outliers if their velocities were more than two standard

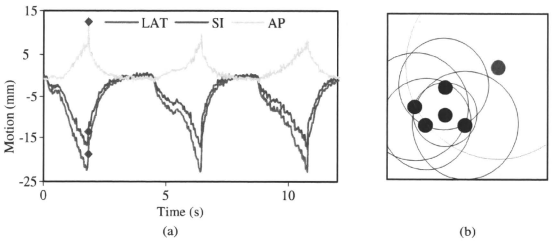

Figure 2. Outlier identifications. (a) An example of an outlier based on velocity: the instantaneous velocity of the tumour at 1.8 s (the three ♦ markers, one for each motion direction) is 4.54 standard deviations above the mean velocity in this treatment session. (b) A simplified example of an outlier based on density, where the circles enclose the nearest four points. The radius of the red/dashed circle is 1.9 standard deviations greater than the mean radius.

deviations above the mean velocity, where the mean and standard deviation are calculated by equations (1) and (2). Figure 2(a) shows a point near 2 s that is an outlier due to its high velocity:

$$\mu = \frac{1}{N-1}\sum_{i=2}^{N}\frac{\vec{r}_i - \vec{r}_{i-1}}{30\,s} \tag{1}$$

$$\sigma = \sqrt{\frac{\sum_{i=1}^{N}(\upsilon_i - \mu)^2}{N-1}}. \tag{2}$$

Density-based outlier removal. The second metric considered the 3D spatial density of the data points. For each data point, the ten closest data points were identified. The density of that data point was then described by the Euclidean distance from the point of interest to its tenth closest neighbour. A data point was identified as an outlier if its density measure was more than 1.8 standard deviations above the mean density measure of all data points in that fraction. In figure 2(b), the red data point is classified as an outlier due to its high density measure. These metrics corresponded well with a visual identification of outliers.

The exclusion of outliers is consistent with other prediction experiments (McCall and Jeraj 2007, Ren *et al* 2007).

(ii) Convex hull creation. After outlier removal, a convex hull was created about the remaining points and its volume calculated using the QHull algorithm implemented by the 'convhull' function in MatLab (Barber *et al* 1996). The volume of the convex hull for each treatment fraction was calculated. The tumour motion space was approximated as a convex hull because convex hulls are of minimally enclosing, well-defined shape that are computationally inexpensive and can relate the position of the fiducial marker at all times of the position sample set. The inter-fractional volumetric changes for each patient can be analysed by monitoring the convex hull volume change from one fraction to another.

In addition, the shapes of the convex hulls can be visually inspected. Several common convex hull shapes were discovered and mapped to the motion space of each fraction. This led to lung tumour motion classification based on the shapes of the motions space. For most

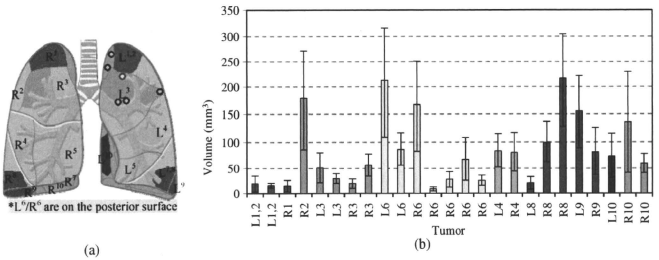

Figure 3. Site-specific volumetric change. (a) The shaded areas indicate the locations of free tumours, while circles indicate tumours that are attached to another structure (table 1). (b) Volumes of the convex hulls averaged over all the treatment fractions of free tumours (i.e. unattached). Error bars indicate the standard deviation.

of the fractions, a convex hull captured the motion space well. However, for some treatment fractions, motion patterns were better described as concave hulls, as discussed in detail below in section 4.

Kang *et al* (2007) described a similar concept, the IGTV, as the total volume occupied during breathing phases. Their study used 4DCT to discern tumour volumes. Handels *et al* (2007) also calculated motion volume in this manner.

(iii) Geometrical correlation analysis. In this work, each tumour's anatomic location was associated with the following four attributes: the pulmonary broncho-segment, the cranio-caudal location, the ventro-dorsal location and tumour adhesion to the cardiac wall. Combining these anatomic attributes along with tumour respiratory motion patterns enabled efficient tumour motion behaviour analysis and facilitated a better understanding of the anatomic effects on tumour motion.

Tumour locations were first categorized based on the bronchial segments (Sheffield 2009), as illustrated in figure 3(a). The upper apex lung region includes segments $L^{1,2}$ and R^1; the middle lung region includes segments L^3-L^5 and R^2-R^5; the peripheral lung region includes segments $L^{7,8}$-L^{10} and R^7-R^{10}; the whole posterior side of the lung is classified as segments L^6 and R^6. The volumetric changes and shapes of tumour motion were then mapped to the corresponding segments, as shown in figure 3(b). This mapping allowed a location–motion space comparison and determination of a correlation between volumetric variation and tumour location. For each tumour, the average volume of the motion space over all treatment sessions was related to tumour motion. The shape–location comparison was performed for individual treatment fractions. Additionally, the amplitude of motion during each fraction was calculated as the maximum Euclidian distance between two points of the fraction. This was compared to the volume of motion.

3. Results

3.1. Volume versus location results

Based on the geometrical mapping of tumours, the average tumour hull volume for each patient, averaged over all treatment fractions, is calculated and arranged in clusters according to the corresponding lung regions. Tumours located in the upper apex had smaller motion spaces

Table 1. Volume of each attached tumour motion envelope, along with its location and the anatomical structure to which it is attached, where the volume of the enclosing convex hulls is averaged over all treatment fractions of the patient. The uncertainty is the standard deviation. When compared to similarly located free tumours, p-values on the order of 10^{-5} are obtained.

Tumour location	Attached to	Motion space volume (mm^3)
$L^{1,2}$	Aorta	19.3 ± 8.2
$L^{1,2}$	Vertebra & aortic arch	71.0 ± 34.0
L^3	Posterior chest wall	25.7 ± 10.9
L^3	Lateral chest wall	6.5 ± 2.6
L^3	Aorta	58.7 ± 24.7
L^6	Anterior chest wall	30.4 ± 10.8

(median 15.7 mm^3; range 14.9–19.3 mm^3) as indicated by the red columns in figure 3(b). The middle region of the lung had slightly larger motion spaces (median 56.2 mm^3; range 19.5–178.8 mm^3), as indicated by the orange and green columns in figure 3(b). Peripheral tumours had the largest volumes (median 90.6 mm^3; range 20.6–216.6 mm^3), as indicated by the blue, purple and lavender columns in figure 3(b). There was considerable variation among posterior tumours, as indicated by the yellow columns in figure 3(b). For tumours attached to fixed anatomical structures, the motion space was small (these results are not shown in figure 3(b) but are summarized in table 1 instead). Considering location groups, p-values greater than 0.05 were found with t-tests comparing segments L3/R3 with L4/R4 (0.07) and L10 (0.53), L4/R4 with L10 (0.33), L8/R8/L9/R9 with R10 (0.50), and L10 with R10 (0.08). As L6/R6 covers the whole posterior, no t-tests were performed on the data from those segments.

3.2. Shape analysis

Three basic shapes and two hybrid shapes were observed to describe the spaces occupied by the respiratory motion paths of the fiducial markers during the three-cycle windows, as shown in figures 4 and 5. The shapes were inter-fractionally consistent, in general, but some tumours demonstrated a progressive change in the shape of their motion space as the number of treatment fractions advanced, as shown in figure 6.

For roughly half of the treatment fractions (49.8%), the tumours had rod-like motion spaces. Tumours moving accordingly have dominant motion amplitude in one dimension and relatively small ones in the other two dimensions. Figures 4(a) and (b) show an example of rod-like tumour motion. Note in this case that the 3D motion is symmetrical between the inhale state and exhale state over time.

Also prevalent were disc-shaped motion spaces, an example of which is shown in figures 4(c) and (d). When the tumour motion has a phase shift among different directions, especially between the two dominant directions, the motion creates an ellipse with a vacant centre presenting a disc-shaped hull. This shape of hull was seen for tumour motion in 38.3% of treatment fractions.

Lastly, in a small proportion of treatment fractions (6.0%), tumour motion followed an arc trajectory within the enclosing convex hull, as shown in figures 4(e) and (f). The convex hulls presented by this type of tumour motion contain much vacant space, resulting in an increased hull volume occupation. These types of motion spaces may be better described as concave

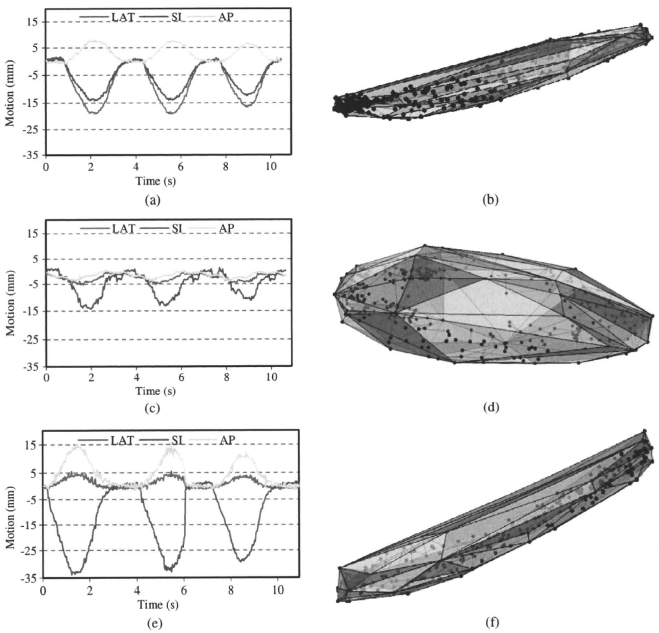

Figure 4. The motion characteristics and the hull shapes, where (a) and (b) are for rod-like hulls, (c) and (d) for disc-shaped hulls and (e) and (f) for arc-shaped hulls.

shapes. The motion versus time plots for tumours in these fractions have thicker tails at the end of exhalation.

Several treatment fractions had convex hulls that could best be described as hybrids of the three basic shapes. One of the more common hybrid shapes apparent in 4.4% of treatment fractions presented as a combination of the disc-shaped and arc-shaped hulls. Observation of the 3D tumour motion over time revealed that there was a phase shift during the late exhalation and a prolonged inhalation peak. This hybrid hull shape encompasses a considerable volume devoid of tumour location points, and so may be better described by a concave enclosure. An example of this hull shape is shown in figures 5(a) and (b).

Another hybrid hull shape for tumour motion that was observed in 1.6% of treatment fractions presented as a combination of rod-like and disc-shaped convex hulls. Also, these tumour motion paths were devoid of tumour location points near the hull centre but were distinguished from the elliptical paths of the disc-shaped hulls by their lack of path curvature. The 3D motion over time may be described as a tent function with sharp inhalation peaks, as shown in figures 5(c) and (d).

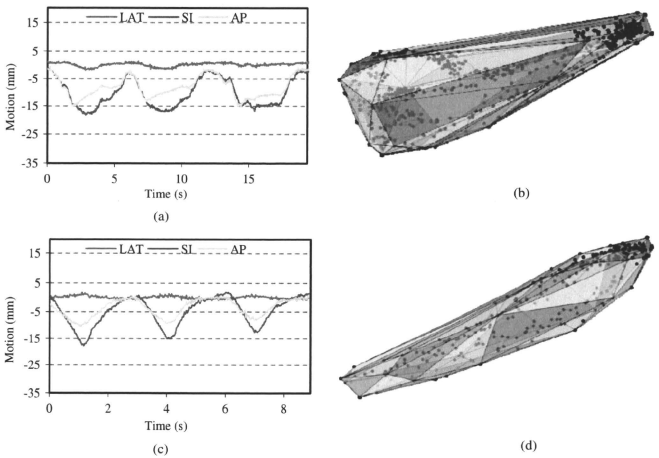

Figure 5. Tumour motion characteristics and hybrid hull shapes. A disc-shaped/arc-shaped hull example is shown in (a) and (b), while a rod-like-disc-shaped hull example is shown in (c) and (d).

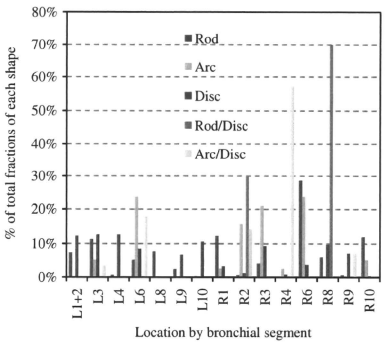

Figure 6. Distribution of motion space shapes normalized for each shape type.

3.3. Shape versus segment results

A comparison of the tumours' motion space shapes and the tumours' geometrical locations is shown in figures 6 and 7. Figure 6 shows that tumours exhibiting rod-like motion hulls were

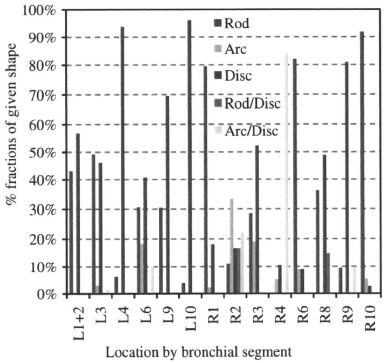

Figure 7. Distribution of hull shapes normalized by bronchial segments.

more likely to be located in the apex, with the exception being segment R^{10}. The hybrid shapes are almost exclusive to the right side of the lung, whereas the general shapes are distributed across both lungs.

For each bronchial segment, all treatment fractions for any tumour at that location have been considered in figure 7. The per cent of fractions of each convex hull shape are calculated, based on the five shapes described above. For example, 82% of fractions in segment R^6 had tumour motion that was enclosed by rod-like hulls, 9% by arc-shaped hulls and 9% by disc-shaped hulls. Results show that elliptical motion is more likely among tumours located in segments L^4, L^9, L^{10} and R^9. Arc paths are slightly more prevalent among tumours located in segments R^2 and R^3.

In a comparison of motion envelope volume and motion amplitude, where amplitude is defined as the maximum distance between any two points of the three breathing cycles for each treatment fraction, the correlation was found to be moderate ($R^2 = 0.602$), see figure 8 and table 2.

4. Discussion

The analysis revealed moderate correlation between tumour location and volume of motion. The comparison of convex hull shape and location was less conclusive. In general, motion increased with proximity to the diaphragm. Hysteresis was present in most locations, but slightly more prevalent in tumours closer to the diaphragm.

When deciding to remove an outlier data point, several considerations were made. The first regarded the data collection. The outlier data points were not identified as being corrupted by mechanical or electronic errors during collection nor were they considered to be noise. The points do, however, represent unlikely physical scenarios. One speculative explanation was coughing by the patient or some other reflex action. This was ruled out because, even with the abrupt change in path and increase in speed expected with a sudden reflex action, with a 30 Hz frame-rate, a trail of points would have been observed instead of the manifestly outlying

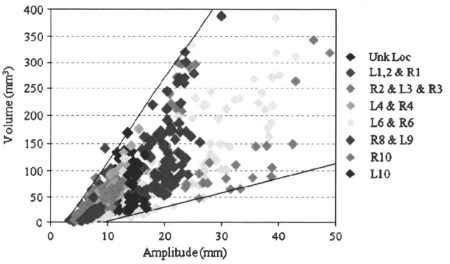

Figure 8. Amplitude versus volume. A comparison of motion amplitude and motion envelope volume. The locations correspond to figure 3(a).

points. A clinical consideration was dosimetry. One measure of the efficacy of a prediction model is its ability to deliver the prescribed dose to the target. The outliers identified in the data for a given treatment fraction substantially increased the size of the prediction space while only representing a fraction of a percentage of the data points. If a prediction model ignored the possibility of the types of outliers seen in the data, the dosimetric consequences would be partial treatment interruptions on the order of 0.1 s per treatment session. This would be negligible when compared to the dosimetric error that would result from a mis-prediction of a second or more.

Several improvements can be made to the volumetric analysis methods. The most useful improvement, as discussed above, would be a volumetric analysis by breathing state. This will involve the identification of breathing state based on the velocity vector of a given data point taken in conjunction with previous data points. Additionally, algorithms to calculate concave volumes would give more representative motion spaces for several of the previously identified shapes. The ability to give accurate concave volumes would also be necessary for the division of motion data into breathing states, especially if any curvature is to be captured. One potential way to do this involves a digitization of the motion data. This could be done by overlaying a 3D grid on the convex hull and including in the concave space any grid location that contains a data point. The ability to precisely calculate the motion space for a tumour at a given state of respiration will greatly enhance the ability to provide accurate predictions of tumour motion. Additional methods being explored include alpha-hulls (Edelsbrunner *et al* 1983) and convex encloses of CT style slices.

The finite-state model for patient respiration allows for four breathing states by the patient: inhaling (IN), exhaling (EX), end of exhalation (EOE) and irregular (IRR) (Wu *et al* 2004). For each state, there are allowable transitions to other states (i.e. IN to EX or IRR, EX to EOE or IRR, EOE to IN or IRR and IRR to any state). Depending on the duration, the patient has been in his or her current state, certain transitions are more likely, giving rise to the notion of a transition probability. The data presented in this article, when coupled with a finite-state model of respiration, may increase the predictive power of the model by identifying the motion space for a particular phase of respiration. Figure 9 illustrates the division of the motion from one treatment fraction into inhalation, exhalation and end of exhalation breathing states. In practice, as implemented in an online tumour tracking system with the predictive model of tumour motion behaviour, the tumour's path may be correlated to the patient's

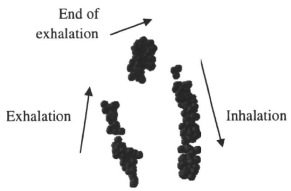

Figure 9. Tumour motion data during the treatment fraction shown in figure 4(d) partitioned according to a finite-state model of patient respiration.

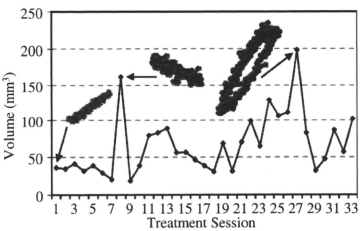

Figure 10. Variation of the tumour motion space size and shape with the increase in the number of treatment fractions. These data were compiled from patient 13 in figure 1 and show a motion space behaviour change from rod-like to disc-shaped.

respiratory state. The respiratory state and tumour motion behaviour may allow for comparison with previous tumours tracked in a data bank so as to identify more probable prediction weightings.

Figure 10 warrants further comment as it reveals an interesting phenomenon. Over the course of treatment, the tumour exhibited larger motion in two dimensions indicating some liberating factor. One possible physiological explanation is that efficacious treatment has reduced the size of the tumour, relieving stress on the patient's airway enabling the patient to breath more deeply. Another possible explanation is that due to changes in tumour size throughout the treatment, the tumour is less constrained in its local environment. Tumour volume data were not tracked throughout the course of treatment and initial volumes were not available for all tumours in the study. This phenomenon was not seen in all patients (ten other tumours showed relative trends of hull volume change at least as large as those shown in figure 10, two of which were volume decreases), but further investigation into the anatomical markers that accompany it may provide clinically useful information. This inconsistency in hysteresis is in line with the poor correlation between amplitude and volume.

The use of shapes to describe classes of motion has the disadvantage of being subjective. The generation of a numerical metric to describe the motion spaces would greatly improve the matching of similar motion spaces for use in the model and permit a determination of degree of similarity. Methods being explored include axial measures and clustering moments. In the

Table 2. Correlation coefficients for figure 8. The locations correspond to figure 3(a).

Location set	R^2
$L^{1,2}$ & R^1	0.451
R^2 & L^3 & R^3	0.853
L^4 & R^4	0.459
L^6 & R^6	0.753
R^8 & L^9	0.536
R^{10}	0.562
L^{10}	0.065
ALL	0.602

absence of such methods, geometric shape is a good surrogate for the similarity of tumour motion behaviour.

5. Conclusions

The main motivation of this study was to characterize intra-fractional tumour motion for the design of appropriate treatment approaches and the development of a predictive model of lung tumour motion behaviour.

This retrospective study of respiratory-induced lung tumour motion has revealed a correlation between tumour location and its motion behaviour. By looking at three breathing cycles of various lung cancer patients, common motion patterns have been observed and their shape and volume have been related to tumour location. A simple motion envelope was found in 52% of tumours that remained consistent over the course of treatment; these were primarily located near the apex of the lung. Conversely, motion envelopes showed large variation for tumours more centrally and inferiorly located. The findings from this study will be used in the development of a model for motion prediction based on a finite state model of patient respiration. Being able to identify the physical space the tumour may occupy during a respiration cycle or in a given phase of respiration considerably increases the potential predictive power for such a model.

Acknowledgment

This research was partially supported by NIH grant 1 R21 CA130849-01.

References

Barber C B, Dobkin D P and Huhdanpaa H T 1996 The quickhull algorithm for convex hulls *ACM Trans. Math. Softw.* **22** 469–83

Bortfeld T, Jokivarsi K, Goitein M, Kung J and Jiang S B 2002 Effects of intra-fraction motion on IMRT dose delivery: statistical analysis and simulation *Phys. Med. Biol.* **47** 2203–20

Chang J, Dong L, Liu H, Starkschall G, Balter P, Mohan R, Liao Z, Cox J and Komaki R 2008 Image-guided radiation therapy for non-small cell lung cancer *J. Thoracic Oncology* **3** 177–186

Chol B, Suh Y, Dieterich S and Keall P 2008 A monoscopic method for real-time tumour tracking using combined occasional x-ray imaging and continuous respiratory monitoring *Phys. Med. Biol.* **53** 2837–55

Edelsbrunner H, Kirkpatrick D G and Seidel R 1983 On the shape of a set of points in the plane *IEEE Trans. Inf. Theory* **29** 551–9

Haasbeek C *et al* 2007 Impact of audio-coaching on the position of lung tumors *Int. J. Radiat. Oncol. Biol. Phys.* **71** 1118–23

Handels H, Werner R, Schmidt R, Frenzel T, Lu W, Low D and Ehrhardt J 2007 4D medical image computing and visualization of lung tumour mobility in spatio-temporal CT image data *Int. J. Med. Inform.* **765** S433–9

Hashimoto T *et al* 2005 Real-time monitoring of a digestive tract marker to reduce adverse effects of moving organs at risk (OAR) in radiotherapy for thoracic and abdominal tumors *Int. J. Radiat. Oncol. Biol. Phys.* **61** 1559–64

Hoisak J D, Sixel K E, Tirona R, Cheung P C and Pignol J P 2006 Prediction of lung tumour position based on spirometry and on abdominal displacement: accuracy and reproducibility *Radiother. Oncol.* **78** 339–46

Imura M *et al* 2005 Insertion and fixation of fiducial markers for setup and tracking of lung tumors in radiotherapy *Int. J. Radiat. Oncol. Biol. Phys.* **63** 1442–7

Jiang S B, Pope C, Al Jarrah K M, Kung J H, Bortfeld T and Chen G T 2003 An experimental investigation on intra-fractional organ motion effects in lung IMRT treatments *Phys. Med. Biol.* **48** 1773–84

Kang Y *et al* 2007 4D proton treatment planning strategy for mobile lung tumours *Int. J. Radiat. Oncol. Biol. Phys.* **67** 906–14

Katoh N *et al* 2008 Real-time tumor-tracking radiotherapy for adrenal tumors *Radiother. Oncol.* **87** 418–24

Keall P J *et al* 2006 The management of respiratory motion in radiation oncology report of AAPM Task Group 76 *Med. Phys.* **33** 3874–900

Keall P J, Kini V R, Vedam S S and Mohan R 2001 Motion adaptive x-ray therapy: a feasibility study *Phys. Med. Biol.* **46** 1–10

Kitamura K *et al* 2002 Registration accuracy and possible migration of internal fiducial gold marker implanted in prostate and liver treated with real-time tumor-tracking radiation therapy (RTRT) *Radiother. Oncol.* **62** 275–81

Low D A, Parikh P J, Lu W, Dempsey J F, Wahab S H, Hubenschmidt J P, Nystrom M M, Handoko M and Bradley J D 2005 Novel breathing motion model for radiotherapy *Int. J. Radiat. Oncol. Biol. Phys.* **63** 921–9

McCall K C and Jeraj R 2007 Dual-component model of respiratory motion based on the periodic autoregressive moving average (periodic ARMA) method *Phys. Med. Biol.* **52** 3455–66

Nakayama H, Mizowaki T, Narita Y, Noriyuki K, Takahashi K, Mihara K and Hiraoka M 2008 Development of a three-dimensionally movable phantom system for dosimetric verifications *Med. Phys.* **35** 1643–50

Onimaru R *et al* 2005 The effect of tumor location and respiratory function on tumor movement estimated by real-time tracking radiotherapy (RTRT) system *Int. J. Radiat. Oncol. Biol. Phys.* **63** 164–9

Putra D, Haas O C, Mills J A and Burnham K J 2008 A multiple model approach to respiratory motion prediction for real-time IGRT *Phys. Med. Biol.* **52** 1651–63

Ren Q, Nishioka S, Shirato H and Berbeco R 2007 Adaptive prediction of respiratory motion for motion compensation radiotherapy *Phys. Med. Biol.* **52** 6651–61

Ruan D, Fessler J, Balter J and Sonke J 2006 Exploring breathing pattern irregularity with projection-based method *Med. Phys.* **33** 2491–99

Sheffield S 2009 http://www.getbodysmart.com/ap/respiratorysystem/lungs/segments/tutorial.html

Shirato H *et al* 2006 Speed and amplitude of lung tumor motion precisely detected in four-dimensional setup and in real-time tumor-tracking radiotherapy *Int. J. Radiat. Oncol. Biol. Phys.* **64** 1229–36

Shirato H *et al* 2000 Four-dimensional treatment planning and fluoroscopic real-time tumour tracking radiotherapy *Int. J. Radiat. Oncol. Biol. Phys.* **48** 1187–95

Smith R *et al* 2009 Evaluation of linear accelerator gating with real-time electromagnetic tracking *Int. J. Radiat. Oncol. Biol. Phys.* **74** 920–7

Vedam S, Keall P, Docef A, Todor D, Kini V and Mohan R 2004 Predicting respiratory motion for four-dimensional radiotherapy *Med. Phys.* **31** 2274–83

Wu H, Sharp G C, Salzberg B, Kaeli D, Shirato H and Jiang S B 2004 A finite state model for respiratory motion analysis in image guided radiation therapy *Phys. Med. Biol.* **49** 5357–72

Wu H, Sharp G C, Zhao Q, Shirato H and Jiang S B 2007 Statistical analysis and correlation discovery of tumour respiratory motion *Phys. Med. Biol.* **52** 4761–74

Yang D, Lu W, Low D A, Deasy J O, Hope A J and El Naqa I 2008 4D-CT motion estimation using deformable image registration and 5D respiratory motion modelling *Med. Phys.* **35** 4577–90

Int. J. Radiation Oncology Biol. Phys., Vol. 77, No. 5, pp. 1596–1603, 2010

0360-3016/$–see front matter

ELSEVIER

doi:10.1016/j.ijrobp.2009.10.015

PHYSICS CONTRIBUTION

RADIATION PNEUMONITIS AFTER HYPOFRACTIONATED RADIOTHERAPY: EVALUATION OF THE LQ(L) MODEL AND DIFFERENT DOSE PARAMETERS

GERBEN R. BORST, M.D., PHD.,* MASAYORI ISHIKAWA, PH.D.,† JASPER NIJKAMP, M.SC.,* MICHAEL HAUPTMANN, PH.D.,‡ HIROKI SHIRATO, M.D., PH.D.,† GERARD BENGUA, PH.D.,† RIKIYA ONIMARU, M.D.,† A. DE JOSIEN BOIS, R.T.T.,* JOOS V. LEBESQUE, M.D., PH.D.,* AND JAN-JAKOB SONKE, PH.D.*

*Department of Radiation Oncology, The Netherlands Cancer Institute—Antoni van Leeuwenhoek Hospital, Amsterdam, The Netherlands; †Department of Radiology, Hokkaido University School of Medicine, Sapporo, Japan; and ‡Departments of Bioinformatics and Statistics, The Netherlands Cancer Institute—Antoni van Leeuwenhoek Hospital, Amsterdam, The Netherlands

Purpose: To evaluate the linear quadratic (LQ) model for hypofractionated radiotherapy within the context of predicting radiation pneumonitis (RP) and to investigate the effect if a linear (L) model in the high region (LQL model) is used.

Methods and Materials: The radiation doses used for 128 patients treated with hypofractionated radiotherapy were converted to the equivalent doses given in fractions of 2 Gy for a range of α/β ratios (1 Gy to infinity) according to the LQ(L) model. For the LQL model, different cut-off values between the LQ model and the linear component were used. The Lyman model parameters were fitted to the events of RP grade 2 or higher to derive the normal tissue complication probability (NTCP). The lung dose was calculated as the mean lung dose and the percentage of lung volume (V) receiving doses higher than a threshold dose of xGy (V_x).

Results: The best NTCP fit was found if the mean lung dose, or V_x, was calculated with an α/β ratio of 3 Gy. The NTCP fit of other α/β ratios and the LQL model were worse but within the 95% confidence interval of the NTCP fit of the LQ model with an α/β ratio of 3 Gy. The V_{50} NTCP fit was better than the NTCP fit of lower threshold doses.

Conclusions: For high fraction doses, the LQ model with an α/β ratio of 3 Gy was the best method for converting the physical lung dose to predict RP. © 2010 Elsevier Inc.

LQ model, LQL model, Radiation pneumonitis, Hypofractionation.

INTRODUCTION

An increasing number of radiotherapy departments implement hypofractionated radiotherapy (RT) regimens for pulmonary malignant lesions, encouraged by reports of good tumor control and little toxicity. Consequently, clinical questions concerning normal tissue tolerance dose and the possibility of including multiple targets or irradiating larger lung volumes (*e.g.*, applying multiple treatments or irradiation of larger tumors) are important.

For conventional fractionated radiotherapy, the physical dose can be converted into a biological equivalent dose by using the linear quadratic (LQ) model (1, 2). Historically, the strength of the LQ model for conventional fraction doses is twofold. First, it is a simple mathematical model fitting log cell survival data as a function of the dose. Second, this model enables isoeffect calculations of fractionation schemes with different doses per fraction. However, in 1954, Puck *et al.* had already observed that for the high-dose regions the log cell survival was linear (3). As a result, some modifications have been derived from NSCLC cell lines (4) and other tumor cell lines and animal isoeffect data (5). In general, a nonlinear part (LQ) in the low-dose region and a linear (L) part for the high-dose region differentiated by a transition dose (d_T) was proposed (*i.e.*, LQL model) (6). Since clinical data are lacking, the clinical isoeffect calculations by the LQ model at higher fraction doses remains uncertain, as was comprehensively discussed previously (7–11). Using the LQ model with an α/β ratio of 3 Gy, it was observed that the normal tissue complication probability (NTCP) model predicting radiation pneumonitis (RP) after hypofractionated RT was not different than the NTCP model after conventional

Reprint requests to: Jan-Jakob Sonke, Ph.D., Department of Radiation Oncology, The Netherlands Cancer Institute—Antoni van Leeuwenhoek Hospital, Plesmanlaan 121, 1066 CX Amsterdam, The Netherlands. Tel: +31-20-5122125; Fax: + 31-20-6691101; E-mail: j.sonke@nki.nl

This work has been supported by a UICC International Cancer Technology Transfer Fellowship and a Grant-in-aid from the Japanese Ministry of Education, Culture, Sports, Science, and Technology.

Supplementary material for this article can be found at www.redjournal.org.

Conflicts of interest: none.

Received May 18, 2009, and in revised form Sept 29, 2009. Accepted for publication Oct 7, 2009.